2025 IEEE World Haptics Conference (WHC)
Suwon Convention Center, Suwon, Korea
July 8 ~ 11, 2025

The Impact of Palpation Motion on Capturing Lumps in Tissue with a Force Sensor

Anzu Kawazoe
Department of Mechanical Engineering
Texas A&M University
Texas, USA
anzutamu@tamu.edu

Pijuan Yu
Department of Mechanical Engineering
Texas A&M University
Texas, USA
pijuanyu@tamu.edu

Thomas Ferris
Industrial & Systems Engineering
Texas A&M University
Texas, USA
tferris@tamu.edu

Rebecca F. Friesen
Department of Mechanical Engineering
Texas A&M University
Texas, USA
rfriesen@tamu.edu

M. Cynthia Hipwell
Department of Mechanical Engineering
Texas A&M University
Texas, USA
cynthia.hipwell@tamu.edu

***Abstract*—Medical palpation is a vital diagnostic technique where practitioners assess a patient's condition through tactile examination. Advancements in remote health technologies should emphasize supporting tactile/haptic modalities to enable some aspects of physical examination to be conducted at a distance. In thyroid examinations, differentiating nodule sizes is critical for identifying malignant lumps.**

This study investigates how palpation motion affects the sensing performance of single-point normal force sensors in detecting thyroid nodules. Using a phantom skin model with lumps of varied sizes and depths, force data was captured and visualized as a stiffness distribution (tactile imaging). The captured lump shapes were compared to actual shapes using Correlation Coefficient (CC), Mean Squared Error (MSE), and Structural Similarity Index (SSIM) methods.

Results showed that single-point normal force sensors effectively detect lumps, particularly during typical palpation motions such as Poke and Push & Pull, with Poke consistently yielding superior performance across various sizes and depths. However, estimating lump shapes becomes increasingly challenging as lump depth increases, regardless of the motion applied. These findings emphasize the importance of motion in optimizing single-point sensors for palpation and provide valuable insights for developing sensorized gloves for clinical use, particularly in remote healthcare systems.

***Index Terms*—Palpation, Tactile imaging, Force sensing, Remote health, Thyroid examination.**

I. Introduction

Palpation is a fundamental component of routine medical examinations, serving as a critical tool for diagnosing a wide range of physiological and pathological conditions [1]. This technique relies on the practitioner's ability to interpret complex sensory inputs, primarily through the sense of touch [2]. Mastery of palpation requires extensive training and refined skills, as it involves assessing tissue texture, consistency, and deformability to detect abnormalities such as lumps, nodules, or areas of tenderness. Traditionally, palpation has been a hands-on procedure, forming a vital link between clinical observation and diagnostic decision-making [3].

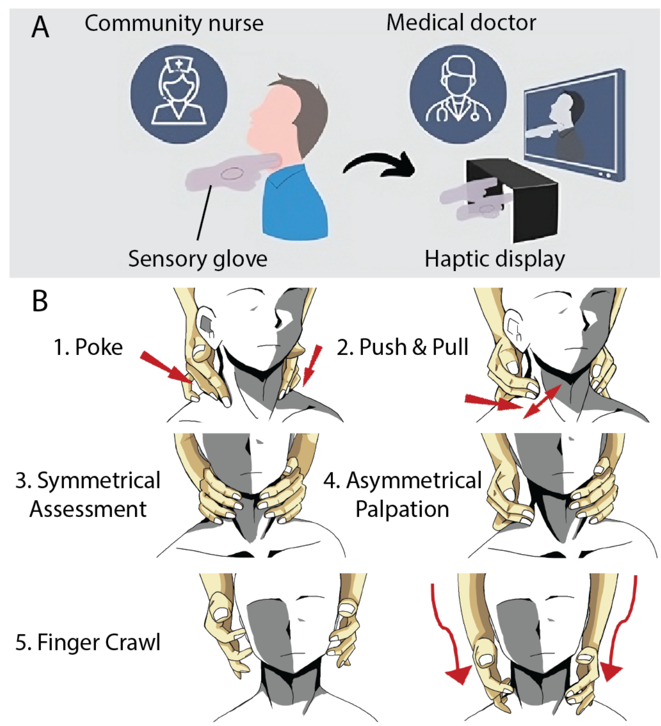

Fig. 1. A) Proposed remote health technology designed to address the shortage of medical doctors. In a medical examination, a community nurse wears a sensory glove to capture haptic sensations, which are transmitted to a medical doctor at a remote location. B) Five major palpation techniques for thyroid examination, identified from the analysis of 10 instructional videos intended for medical students.

Despite its significance, the hands-on nature of palpation presents notable accessibility challenges, particularly for patients who are homebound or reside in remote areas with limited access to healthcare providers. These barriers often result in delayed diagnoses, exacerbating healthcare inequities. While telehealth has successfully addressed many aspects of healthcare accessibility, it struggles to replicate the tactile feedback essential to palpation. This limitation underscores the need for innovative approaches to supplement or replace the tactile components of traditional palpation, ensuring diagnostic capabilities are both accessible and effective.

One promising solution to this challenge is the development of sensorized gloves. Such devices would enable community nurses to perform palpation while capturing detailed tactile data, which could then be transmitted to remote physicians for evaluation (Fig. 1). This approach supports collaborative diagnostics, preserving the critical tactile aspect in telehealth contexts. For practical application, the ability to distinguish lumps of varying sizes, stiffness, shapes, textures, and mobility is essential. Detecting smaller lumps, which are often more likely to be malignant—particularly in thyroid examinations—is of particular importance [4]. Sensorized gloves offer a potential pathway to bridge the gap between hands-on palpation and telehealth, enhancing both diagnostic accuracy and accessibility.

Previous research has demonstrated the feasibility of using force sensors to detect lumps within tissues. For instance, Li et al. developed an arrayed capacitive tactile sensing device capable of capturing lumps with high resolution [5]. Their device evaluated lump detection by applying pressure to the surface of phantom tissue in a static condition. In contrast, Beccani et al. [6] designed a wireless palpation probe, which was mounted on a laparoscopic grasper and actively moved across the liver's surface to map stiffness and identify lumps. Similarly, Li et al. [7] employed a tri-axial force sensor mounted on a robotic arm to detect lumps within phantom tissue. However, research exploring the effects of palpation motion or comparing the effectiveness of different sensor movements for lump detection is limited.

Tactile exploratory motion, a key component of human touch, is effective in perceiving various object properties [8]. For instance, employing multiple exploratory behaviors during robotic tactile exploration significantly improved surface recognition compared to using a single behavior [9]. Thus, understanding the sensing performance under different palpation motions is crucial for optimizing lump detection.

In this study, we investigate how variations in touch motion affect the sensing acuity of a normal-direction force sensor while mimicking palpation motion in thyroid examinations. Specifically, we address the research question: how effectively can a single normal force sensing device capture lumps under different palpation motions? Our goal is to determine whether touch motion influences sensing performance in lump detection. To this end, we created phantom skin, captured force data and displayed it under three distinct motions, visualized the stiffness distribution as tactile imaging, and analyzed which motion most effectively captured lump shapes. While this approach does not involve active human touch, using a robotic system ensures consistent conditions by excluding individual differences such as finger size, damping, touch habits, and posture. This study aims to identify current limitations of single normal-direction sensors in palpation motions and to provide insights for designing sensorized gloves or systems for use in both human and humanoid robot palpation.

II. Background

Our remote healthcare system focuses on thyroid examinations as a model system, particularly on the detection and assessment of thyroid nodules. A thyroid nodule refers to a small mass in the thyroid gland located at the front of the neck. While most nodules are benign, some can be malignant, necessitating further diagnostic tests to determine whether treatment is required [10]. Clinical studies report that thyroid nodules typically range from 5 to 88 mm in diameter [11], with depths ranging from 4 to 25 mm within the tissue [12]. Notably, smaller nodules are more likely to be malignant [4]. These findings highlight the importance of a sensing device with high spatial resolution to detect small and deeply located nodules [5]. Additionally, mobility is critical, as accurately capturing the movement of nodules requires sensors with high spatial and force resolution.

Several wearable technologies have been developed for lump detection in healthcare applications. For example, Li et al. introduced an arrayed capacitive tactile sensing device capable of capturing lumps with high resolution [5], while Pompilio et al. developed a wearable sensor to detect nodules and identify anomalies in bones and rigid structures [13]. The applied force and hand movements during palpation can vary significantly depending on the area being examined and the type of examination [14]. However, insights gained from sensing methods optimized for one region can often be applied to other regions or diagnostic scenarios.

Prior research has established the specifications necessary for tactile sensing technologies that aim to replicate the sensory capabilities of the human hand. To emulate human touch, a response time of 1 ms (equivalent to a 1000 Hz response rate) is required [15]. Force sensing resolution should range from 0.001 N to 0.085 N [16], with a force detection range spanning 0.01 N to 10 N [17]. Spatial resolution should range between 1 mm and 2 mm on a fingertip [18], [19]. The required force ranges vary depending on the type of touch interaction. Additionally, the human hand senses both normal force (perpendicular to the surface) and shear force (parallel to the surface) [20]. These two force components are integral to haptic feedback systems, enhancing the perception of surface shapes and geometries [21], [22]. The accuracy of force sensor measurements is influenced not only by sensor specifications but also by motion dynamics, including acceleration, velocity, and dynamic forces [23], [24].

For evaluating lump detection beneath the skin and tissue, mechanical imaging and stiffness distribution visualization—collectively referred to as tactile imaging—are widely utilized [5]–[7], [25]. Li et al. compared stiffness visualization obtained using their sensor with that from other commercially available high-resolution sensors to validate their device's ability to detect lumps [7]. Beccani et al. also visualized pressure distribution and mechanical imaging to assess lump detection efficacy [6]. Both studies captured lumps during motion, with Li et al. specifically examining lumps of varying sizes (4–10 mm) at different depths in phantom tissue. They visualized these findings using tactile imaging under varied sensing depths [5]. In their approach, the sensor was placed beneath the tissue, and homogeneous indentation was applied from above. The static, arrayed sensor structure captured the lump effectively.

However, a question remains: if a single-point sensor moves across the tissue, can it detect lumps? Furthermore, how do different movement patterns influence lump detection? These questions motivate further exploration of dynamic sensing methods for improved lump detection.

III. Measurement of Tactile Imaging for Detecting Lumps

This study investigates how different sensor movements affect lump detection by recording force data and creating tactile images to evaluate detection effectiveness.

A. Apparatus

Figure. 2 illustrates the complete setup of the force-capturing system. The system consists of a motorized stage, a force sensor (SingleTact Miniature Force Sensor, PPS UK Ltd), and Web cameras (LogitechBRIO webcam, Logitech). The motorized stage can move along the XYZ axes, and the force sensor is attached to the tip of a fixed wand. The scanning wand consisted of a 10 mm diameter flat tip, with an 8 mm SingleTact force sensor mounted centrally. This configuration approximates the average size of a human fingertip contact areas [26].

The phantom skin is placed on the motorized stage, which moves to bring the skin into contact with the sensor tip, simulating palpation motion. Unlike a robotic hand actively engaging with the phantom skin, this setup eliminates biases related to finger posture and other sensor noise issues, such as wiring artifacts. Thus, the fixed sensor and wand setup were employed to focus purely on comparing sensing resolutions under different movements.

The motorized stage and position tracking system are similar to those of Yu et al. [27]. The motorized stage, XYZ translation stage (FSL40, Fuyu Technology Co., China), includes three Nema 17 stepper motors (BE069-3, Befenybay) that provide a resolution of 0.011625 mm per step. We input the trajectory in a Python based software on a PC, and with serial communication, input trajectory is converted to the displacement in an Arduino Due micro controller. The motor divers (DM542T, OMC Corporation Limited, China) control the stage based on the signal from Arduino.

The sensor's location is tracked using a RGB Web camera (Logitech BRIO webcam, Logitech) that detects a green marker placed on the sensor. Three web cameras simultaneously capture the marker's position to determine its X, Y, and Z coordinates using a YUV colorspace tracking algorithm supported by OpenCV [28]. The force sensor readings and the marker's X, Y, and Z positions are recorded simultaneously at a frequency of 60 Hz. The resolution of the position tracking is 0.3 mm in X, Y, Z position.

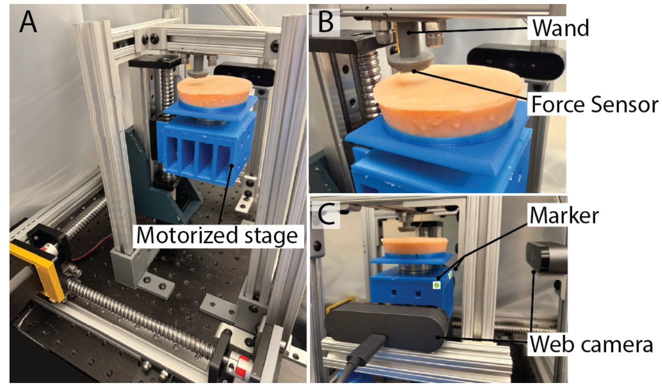

Fig. 2. A) The three-axis motorized stage enables the force sensor to make contact with the phantom skin using three different movement patterns. B) A force sensor is mounted at the tip of the wand, which is designed to mimic the shape of a fingertip. C) Three web cameras track the position of the stage by monitoring green markers located on the two sides and the top of the blue stage. Each web camera tracks a each green marker.

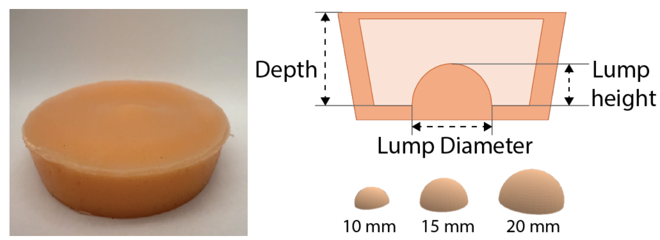

Fig. 3. The phantom skin used for this measurement. The surface, edge, and lump are made of Ecoflex, while the interior is filled with soft slime to mimic the tactile sensation of tissue. Details of the fabrication process are provided in a previous research project by Yu et al. [27]. There are two depth 11 mm and 20 mm and in each depth of phantom skin, 10, 15, 20 mm diameter of lump is included in the phantom skin

The SingleTact force sensor used in this study has an 8 mm diameter and a 0.3 mm thickness. It measures normal forces with resolutions of 0.02 N and supports force ranges of -5 to 10 N. In tactile interactions, human hands typically exert a maximum force of approximately 10 N [29]. Medical professionals' palpation characteristics during thyroid examinations show an average applied touch force of around 7 N. The sensor's range of -5 to 10 N, and its high resolution make it well-suited for this study, and the thickness of the sensor does not disturb interaction with the phantom skin in palpation motions when it is attached on a finger pad. Thus, we employed this commercial force sensor (resolution: 0.02 N; range: -5 to 10 N) for the measurements. The captured analog signal from the force sensor is converted by the data acquisition device (NI PCIe-6343, National Instruments, USA) and stored as force [N] with the captured position.

The phantom skin used in this study (Fig.3) mimics human skin, both with and without embedded lumps. This type of phantom is fabricated with same process as previous palpation and haptics research [27]. Based on clinical studies of thyroid examination [11] and input from ENT doctors, lumps are classified as large (greater than 30 mm in diameter), medium (approximately 20 mm in diameter), and small (less than 15 mm in diameter). These are located at average depths of 11 mm and a maximum 20 mm from surface of the skin to the center of the lump. Therefore, for this study, we used lumps of 20 mm, 15 mm, and 10 mm in diameter, positioned at depths of 11 mm and 20 mm from the skin surface to the lump center. The stiffness of the lumps was varied to represent different clinical conditions. To replicate the stiffness of human tissue, the lumps were made using Ecoflex 00-10 (Smooth-On, Inc. PA, USA), the same material used for the skin and edge regions of the phantom tissue. The lumps were fixed at the base during fabrication. To minimize differences in size and thickness, molds were employed during phantom skin fabrication. Additionally, soft gel-like material was filled into the phantom skin to mimic internal body tissue.

B. Identified Palpation Motion

In another study [30], we identified five primary palpation motions (Figure 1B): "Finger Crawl," "Push and Pull," "Poke," "Symmetrical Assessment," and "Asymmetrical Palpation" through the study of 10 palpation instruction videos of thyroid examination and input from ENT doctors. The "Finger Crawl" involves alternating finger movements to explore contours and structures, while "Push and Pull" combines pressure and gliding motions. "Poke" applies direct pressure to specific points, and "Asymmetrical Palpation" uses one hand for anchoring while the other performs dynamic movements. "Symmetrical Assessment" compares corresponding sides of the body. Instead of capturing force under all palpation motions, "Push and Pull" and "Poke" motions were selected because they are compositional components of more complex clinical motions such as "Symmetrical Assessment," "Asymmetrical Palpation," and "Finger Crawl" [30]. Clinical observation and physician feedback indicate "Push and Pull" and "Poke" are employed independently and serve distinct diagnostic purposes.

C. Tactile Imaging Measurement

The moving stage operates based on the specified trajectory input. In this study, we measure the force generated during three distinct movement patterns, designed to mimic "Trace," "Poke," and "Push-and-Pull" hand motions. These movements are referred to as Controlled Sliding, Poke, and Push & Pull throughout this paper. Controlled Sliding, though not standard in thyroid examinations, was included for comparison. The trajectories for these movements are illustrated in Fig. 4. The moving stage travels at a speed of 18 mm/s for all trajectories.

In the Controlled Sliding motion, the sensor first indents to a depth of 7 mm (for 11mm depth of phantom skin) or 19 mm (for 20 mm depth of phantom skin) and follows the trajectory at this depth. Force data is captured at 1 mm intervals along the trajectory to create a tactile image (Fig. 4A). In the Poke movement, the sensor intermittently indents the surface by 7 mm/19 mm mm at each 1 mm interval along the trace trajectory (Fig. 4B). Force measurements are recorded at the

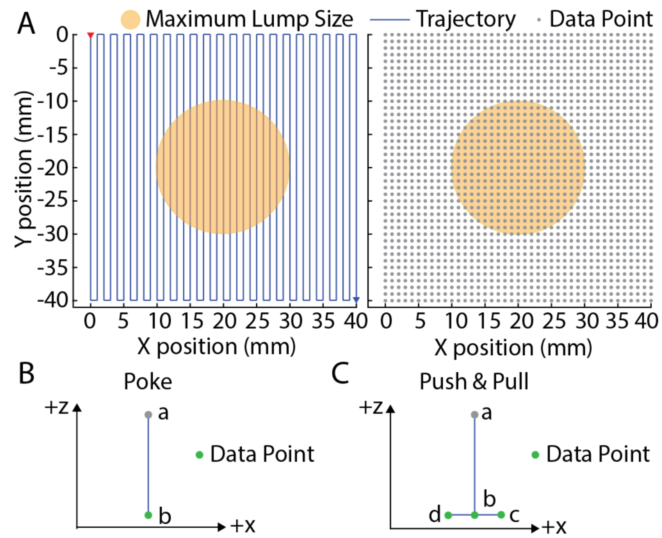

Fig. 4. A) (Left) In the Controlled Sliding motion, the trajectory of the stage begins at the red point and follows the blue line. (Right) During the movement, force data is collected at the gray dots. B) In the Poke motion, at each gray dot shown in A (Right), the sensor position indents from point a to point b. During the movement, force data is collected at the green dots. C) In the Push & Pull motion, the sensor position follows the sequence of a → b → c → d → b → a at each gray dot in A (Right). During the movement, force data is collected at the green dots.

7 mm/19 mm mm depth during each poke to construct the tactile image. For the Push & Pull movement, the sensor alternates between indenting 7 mm/19 mm mm and moving horizontally by 2 mm (Fig. 4C). Force data is collected during the horizontal movement at the same 7 mm/19 mm indentation depth to render the tactile image. Indentation depths of 7 mm and 19 mm were selected to reach the approximate center of the embedded lumps, based on preliminary testing. These values correspond to realistic interaction depths found in thyroid palpation. The 7 mm indentation ensured effective contact for 11 mm-deep lumps, while deeper indentation (19 mm) was required for 20 mm-deep lumps to overcome soft tissue attenuation.

D. Analysis and Evaluation Methodology

To evaluate the performance of the force sensor in detecting lumps embedded in phantom skin, we employed a methodology that compared stiffness maps, derived from captured force distribution, to reference hemispherical shapes which are lump shapes. The analysis began with the collection of force distribution data, which was centered within a 20 mm × 20 mm area. These force distributions were converted to stiffness maps (tactile imaging) using the relationship $k = \frac{F}{x}$, where F represents the measured force and x is the constant displacement from the original skin surface to the sensing point. Reference shapes were modeled as hemispheres with diameters of 10 mm, 15 mm, and 20 mm, truncated at a height of 4 mm (in Phantom skin depth of 11 mm) or 1 mm (in Phantom skin depth of 20 mm) from the base to match the sensor's detection range. These truncated hemisphere heights were converted to a heat map which is the same resolution as

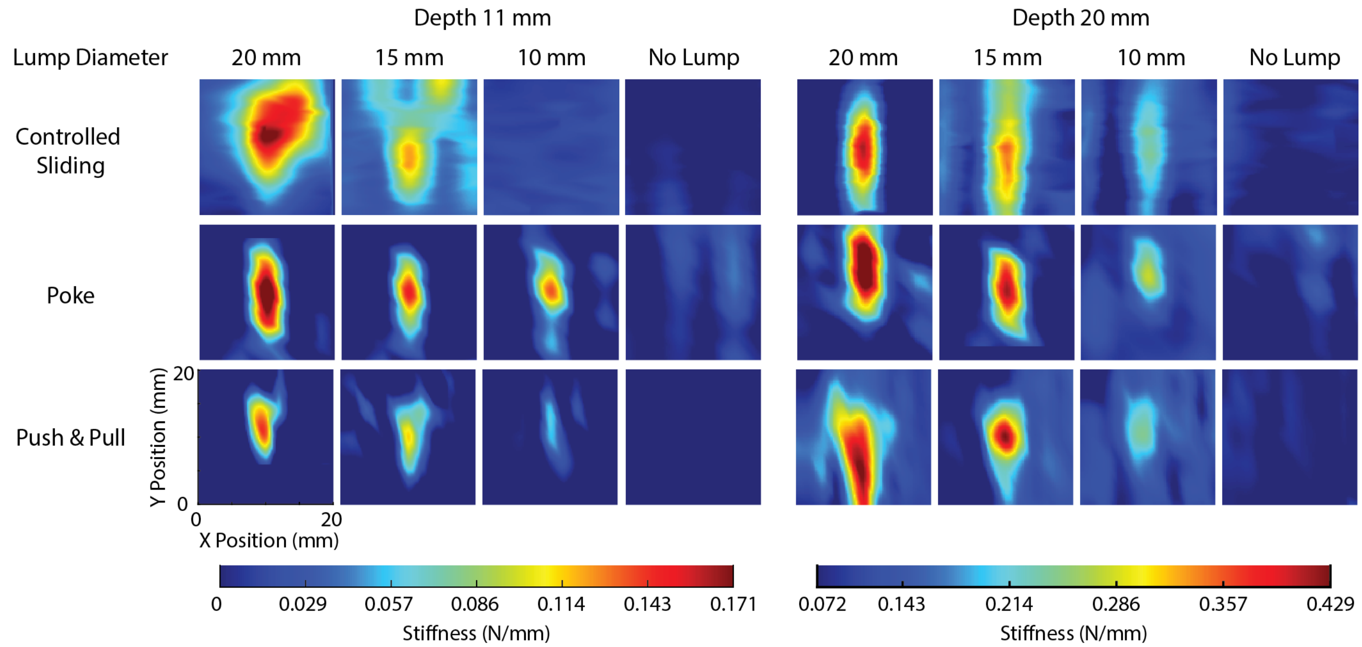

Fig. 5. The tactile imaging represents the stiffness distribution in the X, Y position obtained from force measurements across 20 mm, 15 mm, 10 mm lumps, and a no-lump condition. Measurements were captured under three different sensing point movements (Controlled Sliding, Poke, and Push & Pull) with depths of 11 mm and 20 mm of the phantom skin. All tactile imaging results are trimmed to a 20 × 20 mm square. The color bar indicates stiffness values. For a depth of 11 mm, the sensing point indentation is 7 mm across all movements, while for a depth of 20 mm, the sensing point indentation is 19 mm.

the tactile imaging and served as the ground truth for comparison with the tactile images. Each tactile image was interpolated onto the reference shape's grid to ensure precise alignment. To evaluate the similarity between reconstructed and ground truth lump shapes, we selected three complementary metrics: Correlation Coefficient (CC), Mean Squared Error (MSE), and Structural Similarity Index (SSIM). These were chosen because CC captures spatial pattern similarity, MSE provided a measure of absolute error, and SSIM assesses similarity by analyzing structural consistency between the tactile imaging and the heat map of reference shapes. They are widely used in medical and tactile image analysis [31]–[35]. The combined use of these metrics offered a comprehensive assessment of sensor performance. CC highlighted spatial alignment, but it did not account for magnitude or structural errors. MSE emphasized accuracy in stiffness magnitude but was sensitive to outliers. SSIM complemented these by capturing structural fidelity, although it could overlook quantitative magnitude errors. By integrating these metrics, we achieved a balanced evaluation of spatial accuracy, magnitude fidelity, and structural similarity, providing a robust framework to validate the sensor's capability in detecting and characterizing embedded lumps.

IV. Result

The aim of this study is to investigate how sensing motions influence the capture of lumps in phantom skin. Lumps in phantom skin were captured using three different motions. Figure 5 illustrates tactile imaging, which visualizes the stiffness distribution of varied lump sizes at different depths under the three motion conditions. In the tactile images, regions of higher stiffness indicate the captured lumps within the phantom skin. For a lump at a depth of 11 mm, the lump is visible in the tactile images when using the controlled sliding motion (18 mm/s) and under other conditions as well. For a lump at a depth of 20 mm, the captured lump remains discernible under all three motion conditions.

To further examine how accurately the captured lump resembles the actual lump geometry, we evaluated the sensing performance under the three motions—Controlled Sliding, Poke, and Push & Pull—using tactile images to represent captured lumps in phantom skin. The comparison with heat map of actual lump shape at the sensing point was conducted using three metrics: Correlation Coefficient (CC), Mean Squared Error (MSE), and Structural Similarity Index (SSIM). The metric values for all lump sizes under the three motion conditions are summarized in Table I (for a depth of 11 mm) and Table II (for a depth of 20 mm). The evaluation criteria were as follows: CC values closer to +1 indicate a strong positive correlation, minimal MSE reflects higher accuracy, and higher SSIM values signify closer similarity to the actual lump geometry. Conversely, CC values close to 0 or negative indicate poor correlation.

V. Discussion

As shown in the tactile imaging results (Fig. 5), with palpation motions such as Poke and Push & Pull, a single normal-direction force sensor successfully detected lumps measuring 20 mm, 15 mm, and 10 mm in diameter at depths of 11 mm and 20 mm within the phantom skin. According to a previous clinical study [12] and feedback from physicians, the average depth of thyroid nodules is approximately 11 mm, with a maximum depth of 20 mm. Additionally, lumps smaller than 15 mm are typically classified as small. These findings suggest that when a normal-direction force sensor is used during palpation motions, detecting lumps is feasible in most thyroid nodule cases.

In Fig. 5, the reconstructed shapes appeared narrower in the x-direction. We hypothesize this may be due to anisotropic deformation in the phantom tissue during scanning. Specifically, motion-induced lateral tissue drag could lead to shape skewing depending on the scanning axis.

When evaluating how accurately the detected lump geometry resembled the actual lump, the Poke motion demonstrated superior performance at a depth of 11 mm. It achieved the highest positive correlation coefficients (CC) across all lump sizes, the lowest mean squared error (MSE) for the 10 mm lump, and the highest structural similarity index measure (SSIM) for the same size. While the MSE values were similar across all motions, the Controlled Sliding motion consistently showed negative CC values, indicating poor correlation. The Push & Pull motion performed moderately well but was outperformed by the Poke motion in both CC and SSIM metrics. At a depth of 20 mm, all three motions produced negative CC values. The MSE values were higher, and the SSIM values were lower compared to those at 11 mm. This indicates that while the sensor can physically reach deeper lumps, capturing their shapes becomes more challenging due to the increased thickness of tissue between the lump and the skin, which likely distorts the measurement.

The Controlled Sliding motion, while not part of the standard clinical palpation technique for thyroid examinations, was included for comparative purposes. The results clearly demonstrate why this motion is not used clinically. Across both 11 mm and 20 mm depths, the Controlled Sliding motion yielded negative CC values, higher MSE, and lower SSIM across most lump sizes. These findings indicate that the Controlled Sliding motion results in poor resemblance to the actual lump geometry. This is likely due to the lateral motion of the soft tissue and skin during sensor movement, which causes the sensor's contact point to shift. In this study, the sensor tip was designed to mimic a human fingertip. However, during lateral motion, both the skin and the underlying soft lump moved along with the sensor, a phenomenon similar to that observed with actual finger movement. Additionally, lump detection during lateral motion depends heavily on the extent to which the fingertip sinks into the skin to reach the lump. These factors explain why controlled lateral motion is not effective for thyroid examinations.

Overall, the results highlight that the performance of lump shape detection using a single normal-direction force sensor depends on the sensor's motion. Among the tested motions, the Poke motion was the most effective for capturing lump shapes. However, when lumps are located in deeper tissues, accurately capturing their shapes remains challenging. The use of multi-point or multi-directional force sensors with higher resolution could enhance sensing robustness and overcome these limitations. In future studies, we plan to evaluate the sensing performance of these advanced sensors. Furthermore, we aim to investigate how well sensors can capture lump geometry when attached to an actual finger in active touch.

TABLE I

PERFORMANCE METRICS FOR EACH SENSING MOTION ACROSS LUMP SIZES IN 11 MM DEPTH OF PHANTOM SKIN.

Method	Lump (mm)	CC	MSE	SSIM
Controlled Sliding	20	-0.2614	37.4664	0.1467
Controlled Sliding	15	-0.2019	11.1737	0.4769
Controlled Sliding	10	-0.0996	1.4190	0.8032
Poke	20	0.1824	37.4972	0.1569
Poke	15	0.1760	11.1795	0.4869
Poke	10	0.0593	1.4190	0.8150
Push & Pull	20	0.0990	37.5329	0.1495
Push & Pull	15	0.1005	11.1762	0.5057
Push & Pull	10	0.0933	1.4190	0.8039

TABLE II

PERFORMANCE METRICS FOR EACH SENSING MOTION ACROSS LUMP SIZES IN 20 MM DEPTH OF PHANTOM SKIN.

Method	Lump (mm)	CC	MSE	SSIM
Controlled Sliding	20	-0.2652	38.2883	0.0929
Controlled Sliding	15	-0.1594	12.1135	0.3386
Controlled Sliding	10	-0.1004	2.3803	0.5395
Poke	20	-0.2425	38.2941	0.0931
Poke	15	-0.1173	12.0409	0.3353
Poke	10	-0.1237	2.3871	0.5419
Push & Pull	20	-0.1493	38.1515	0.0932
Push & Pull	15	-0.2124	12.1335	0.3376
Push & Pull	10	-0.1618	2.3941	0.5409

VI. CONCLUSION

In this study, we investigated the capability of a single-point normal force sensor to capture the shape of lumps in phantom skin under three types of motions, including those mimicking palpation touch. We generated tactile imaging and evaluated performance using CC, MSE, and SSIM metrics.

The results of the tactile imaging demonstrate that the single-point normal force sensor effectively detects lumps, particularly under typical palpation motions such as Poke and Push & Pull. Notably, the Poke motion consistently performed better in detecting lumps of varying sizes and depths within the phantom skin. Conversely, using a controlled sliding motion—uncommon in clinical palpation for thyroid examination but common in scanning technology—yielded lower performance in capturing lump shapes. These findings highlight the importance of motion in optimizing the performance of single-point normal force sensors during palpation. This knowledge may contribute to the development of sensory gloves designed for clinical palpation, particularly in remote health systems.

ACKNOWLEDGMENT

This work was supported by the US National Science Foundation (NSF-2222918). We thank Dr. Eugene L. Alford, M.D., Dr. Ericka P. Greene, M.D., and Dr. Michael Ferris, M.D., for their valuable comments.

REFERENCES

[1] L. S. Bickley, *Bates' Guide to Physical Examination and History Taking*, 13th ed. Lippincott Williams & Wilkins, 2020.

[2] S. J. Lederman and R. L. Klatzky, "Haptic perception: A tutorial," *Attention, Perception, & Psychophysics*, vol. 71, no. 7, pp. 1439–1459, 2009.

[3] S. J. Reiser, *Medicine and the Reign of Technology*. Cambridge University Press, 1978.

[4] P. W. Wiest, M. F. Hartshorne, P. D. Inskip, L. A. Crooks, B. S. Vela, R. J. Telepak, M. R. Williamson, R. Blumhardt, J. M. Bauman, and M. Tekkel, "Thyroid palpation versus high-resolution thyroid ultrasonography in the detection of nodules." *Journal of Ultrasound in Medicine*, vol. 17, 1998.

[5] B. Li, Y. Shi, A. K. Fontecchio, and Y. Visell, "Mechanical imaging of soft tissues with a highly compliant tactile sensing array," *IEEE Transactions on Biomedical Engineering*, vol. 65, pp. 687–697, 2018.

[6] M. Beccani, C. D. Natali, L. J. Sliker, J. A. Schoen, M. E. Rentschler, and P. Valdastri, "Wireless tissue palpation for intraoperative detection of lumps in the soft tissue," *IEEE Transactions on Biomedical Engineering*, vol. 61, pp. 353–361, 2014.

[7] L. Li, B. Yu, C. Yang, P. Vagdargi, R. A. Srivatsan, and H. Choset, "Development of an inexpensive tri-axial force sensor for minimally invasive surgery," *2017 IEEE/RSJ International Conference on Intelligent Robots and Systems (IROS)*, pp. 906–913, 2017.

[8] S. J. Lederman and R. L. Klatzky, "Hand movements: A window into haptic object recognition," *Cognitive Psychology*, vol. 19, no. 3, pp. 342–368, 1987.

[9] J. Sinapov, V. Sukhoy, R. Sahai, and A. Stoytchev, "Vibrotactile recognition and categorization of surfaces by a humanoid robot," *IEEE Transactions on Robotics*, vol. 27, pp. 488–497, 2011.

[10] H. A. Al-Hakami, R. Alqahtani, A. Alahmadi, D. Almutairi, M. Algarni, and T. A. Alandejani, "Thyroid nodule size and prediction of cancer: A study at tertiary care hospital in saudi arabia," *Cureus*, vol. 12, 2020.

[11] M. J. Magister, I. Chaikhoutdinov, E. W. Schaefer, N. Williams, B. Saunders, and D. M. Goldenberg, "Association of thyroid nodule size and bethesda class with rate of malignant disease." *JAMA otolaryngology–head & neck surgery*, vol. 141 12, pp. 1089–95, 2015.

[12] X. Xie and Y. Yu, "Effect of the location and size of thyroid nodules on the diagnostic performance of ultrasound elastography: A retrospective analysis," *Clinics*, vol. 75, 2020.

[13] M. Pompilio, N. D'Aurizio, T. L. Baldi, L. Franco, G. Gabriele, and D. Prattichizzo, "A novel wearable sensing device enabling remote palpation," *2024 IEEE Haptics Symposium (HAPTICS)*, pp. 149–156, 2024.

[14] N. Wang, G. J. Gerling, R. M. Childress, and M. L. Martin, "Quantifying palpation techniques in relation to performance in a clinical prostate exam," *IEEE Transactions on Information Technology in Biomedicine*, vol. 14, pp. 1088–1097, 2010.

[15] A. Simpkins, "Robotic tactile sensing: Technologies and system (dahiya, r.s. and valle, m.; 2013) [on the shelf]," *IEEE Robotics & Automation Magazine*, vol. 20, pp. 107–107, 2013.

[16] R. S. Johansson, Å. B. Vallbo, and G. Westling, "Thresholds of mechanosensitive afferents in the human hand as measured with von frey hairs," *Brain Research*, vol. 184, pp. 343–351, 1980.

[17] P. Dario, *Tactile sensing for robots: present and future*. Cambridge, MA, USA: MIT Press, 1989, p. 133–146.

[18] R. S. Dahiya, G. Metta, M. Valle, and G. Sandini, "Tactile sensing—from humans to humanoids," *IEEE Transactions on Robotics*, vol. 26, pp. 1–20, 2010.

[19] M. H. Lee, "Tactile sensing: New directions, new challenges," *The International Journal of Robotics Research*, vol. 19, pp. 636 – 643, 2000.

[20] G. Robles-De-La-Torre and V. Hayward, "Force can overcome object geometry in the perception of shape through active touch," *Nature*, vol. 412, pp. 445–448, 2001.

[21] A. Girard, M. Marchal, F. Gosselin, A. Chabrier, F. Louveau, and A. Lécuyer, "Haptip: Displaying haptic shear forces at the fingertips for multi-finger interaction in virtual environments," *Frontiers ICT*, vol. 3, p. 6, 2016.

[22] M. Sarac, T. M. Huh, H. Choi, M. R. Cutkosky, M. D. Luca, and A. M. Okamura, "Perceived intensities of normal and shear skin stimuli using a wearable haptic bracelet," *IEEE Robotics and Automation Letters*, vol. 7, pp. 6099–6106, 2019.

[23] B. Sundaralingam, A. Lambert, A. Handa, B. Boots, T. Hermans, S. Birchfield, N. D. Ratliff, and D. Fox, "Robust learning of tactile force estimation through robot interaction," *2019 International Conference on Robotics and Automation (ICRA)*, pp. 9035–9042, 2018.

[24] Z. Wang, X. Zhang, and M. Li, "Accuracy analysis and experimental study of a six-dimensional force sensor with circular flexible spherical joints," *Sensors (Basel, Switzerland)*, vol. 23, 2023.

[25] J. C. Gwilliam, Z. Pezzementi, E. Jantho, A. M. Okamura, and S. Hsiao, "Human vs. robotic tactile sensing: Detecting lumps in soft tissue," in *2010 IEEE Haptics Symposium*, 2010, pp. 21–28.

[26] R. S. Johansson and Å. B. Vallbo, "Tactile sensibility in the human hand: Relative and absolute densities of four types of mechanoreceptive units in glabrous skin," *The Journal of Physiology*, vol. 286, pp. 283–300, 1979. [Online]. Available: https://doi.org/10.1113/jphysiol.1979.sp012619

[27] P. Yu, L. C. Batteas, T. Ferris, M. C. Hipwell, F. Quek, and R. F. Friesen, "Investigating passive presentation paradigms to approximate active haptic palpation," *IEEE Transactions on Haptics*, 2024.

[28] G. Bradski, "The opencv library," *Dr. Dobb's Journal of Software Tools*, 2000.

[29] R. S. Dahiya and M. Valle, *Robotic Tactile Sensing: Technologies and System*. Springer Publishing Company, Incorporated, 2014.

[30] A. Chan, A. Kawazoe, N. Kim, R. F. Friesen, T. K. Ferris, F. Quek, and M. C. Hipwell, "Characterization of medical neck palpation to inform design of haptic palpation sensors," *Sensors (Basel, Switzerland)*, vol. 25, p. 2159, 2025.

[31] A. Mason, J. A. Rioux, S. E. Clarke, A. F. Costa, M. H. Schmidt, V. Keough, T. Huynh, and S. D. Beyea, "Comparison of objective image quality metrics to expert radiologists' scoring of diagnostic quality of mr images," *IEEE Transactions on Medical Imaging*, vol. 39, pp. 1064–1072, 2020.

[32] Z. Wang, A. C. Bovik, H. R. Sheikh, and E. P. Simoncelli, "Image quality assessment: from error visibility to structural similarity," *IEEE Transactions on Image Processing*, vol. 13, pp. 600–612, 2004.

[33] Z. Wang and A. C. Bovik, "Mean squared error: Love it or leave it? a new look at signal fidelity measures," *IEEE Signal Processing Magazine*, vol. 26, pp. 98–117, 2009.

[34] U. Sara, M. Akter, and M. S. Uddin, "Image quality assessment through fsim, ssim, mse and psnr—a comparative study," *Journal of Computer and Communications*, 2019.

[35] A. K. Venkataramanan, C. Wu, A. C. Bovik, I. Katsavounidis, and Z. Shahid, "A hitchhiker's guide to structural similarity," *IEEE Access*, vol. 9, pp. 28 872–28 896, 2021.